Central European Journal of Energetic Materials
ISSN 1733-7178; e-ISSN 2353-1843

Cent. Eur. J. Energ. Mater. 2018, *15*(4): 572-589; DOI 10.22211/cejem/100682

Research paper

Fabrication of Nano- and Micron- Sized Spheres of CL-20 by Electrospray

Shi Yan*, Mengyao Li, Lu Sun, Qingjie Jiao, Ronghui Huang

Beijing Institute of Technology, 5 South Zhong Guan Cun Street, Haidian Beijing 100081, P. R. China
**E-mail: ys13@bit.edu.cn*

Abstract: The application of hexanitrohexaazaisowurtzitane (CL-20) in energetic materials will be expanded by its use as superfine particles. A method of fabricating nano- and micron-sized spheres of CL-20 by using electrospray is discussed. The effects of the precursor solution and the experimental conditions on the morphology and the crystal phase of the CL-20 particles are introduced. A variety of solvents was used to dissolve raw CL-20 for the preparation of the precursor solution with different CL-20 contents. The conductivity and viscosity of the precursor solutions were tested before the electrospray process. The electrostatic parameters were adjusted by changing the voltage and the distance between the nozzle and the plate. The morphology, crystal phase, mechanical sensitivity, density, and thermal stability of the raw CL-20 and the as-sprayed CL-20 samples were determined using scanning electron microscopy, X-ray diffraction, and differential scanning calorimetry (DSC). Furthermore, the density and the mechanical sensitivity were tested for the raw and the as-sprayed CL-20. DSC tests were conducted to compare the thermal stability and reactivity of the samples.

Keywords: energetic materials, explosives, CL-20, electrospray, spherical particles

1 Introduction

Hexanitrohexaazaisowurtzitane (CL-20) is a new cage nitramine explosive. Its structure consists of a rigid isowurtzitane cage with a nitro group attached to each of the six bridging nitrogen atoms within the cage. The oxygen balance of CL-20

is −11%, which is higher than that of cyclotetramethylenetetranitramine (HMX) and cyclotrimethylenetrinitramine (RDX). CL-20 also has a higher heat of formation (~ +419 kJ/mol) and a higher density (2.044 g/cm^3) for the ε phase than HMX and RDX. These attributes have been speculated to lead to an approximately 14-20% higher performance than that of HMX [1]. In addition, the higher detonation velocity and pressure of CL-20 make it an appropriate alternative for replacing HMX and RDX in military field applications.

Micron/nanometer sized explosives have attracted increased attention in both industrial and scientific research in recent decades, because nano-explosives exhibit excellent size-dependent properties, including a low ignition temperature and low mechanical sensitivity, and high energy release and detonation velocity. Therefore, the preparation of micron/nanometer sized explosives is a route to obtain an insensitive explosive. Several techniques have been developed to produce nanometer and micrometer sized explosive particles, including mechanical grinding [2], solvent–nonsolvent recrystallization [3], spray drying [4], supercritical fluid recrystallization [5], and the sol-gel method [6]. Compared with these techniques, the process of electrospray is a very simple one-step method that uses little solvent and generates little residue; this results in a remarkable reduction in production costs. Moreover, many materials can be made, but only if the materials can be dispersed in a solvent to form a homogenous solution [7, 8].

Electrospray has been used for the preparation of small particles in many fields [8, 9], including energetic materials containing metal fuels [10, 11]. In the electrospray process, an electrostatic field is applied between the nozzle capillary and the metal ground collector plate, and the precursor liquid flow is injected from the axis of the nozzle. Monodispersed fine droplets are formed when the flow travels towards the collector plate, because of the instabilities resulting from the repulsive force between the surface charges of the droplets. The droplet size can be controlled by adjusting the flow rate and the voltage applied between the syringe nozzle and the collector plate. The diameter of the droplets is of the order of nanometers [12]. The procedure requires no template or surfactants, and can be implemented at ambient temperature and pressure.

This paper describes a novel method for the preparation of nano- and micron-sized spheres of CL-20. The morphologies and size distributions of the particles are greatly influenced by the experimental conditions, which include the properties of the electric field and the precursor solutions *etc.* The as-sprayed CL-20 particles were characterized by SEM, XRD, DSC and sensitivity tests (friction and impact). The results were compared with the raw material CL-20.

2 Experimental

The raw CL-20 powders were purchased from Qingyang Chemical Industry. The crystal phase was ε, and the average particle size was ~150 μm. Acetone and ethyl acetate used as the solvents were analytical reagents purchased from Beijing Chemical Works.

The electrospray arrangement is shown in Figure 1 and consists mainly of a high-voltage supply, a syringe pump, and a collector. In the electrospray process, the precursor solution was injected from a syringe using a micro-syringe pump into the metal needle. The diameter of the metal syringe needle ranged from 0.21 mm to 0.86 mm. The high-voltage power supply provided a varying voltage from 0.5 kV to 50 kV. The two poles were separately connected to the metal needle and the plate to generate a high electric field, which caused charge accumulation on the surface of the solution, forced the droplets to overcome the surface tension, making a cone, called the Taylor cone, at the tip of the nozzle. A jet was then emitted from the apex of the cone. During flight, the jet broke up into droplets because of instabilities caused by the electric field. As the surface charge was increased to a limiting value (the Rayleigh limit), the droplets were disrupted into smaller ones, resulting in a decrease in the surface charge density with an increase in the surface area. The solution concentration increased by evaporation of the solvent. The droplets gradually shrank, which caused the driving force of crystallization to become sufficiently large; nanosized particles were thus formed. The products accumulated on the collector plate.

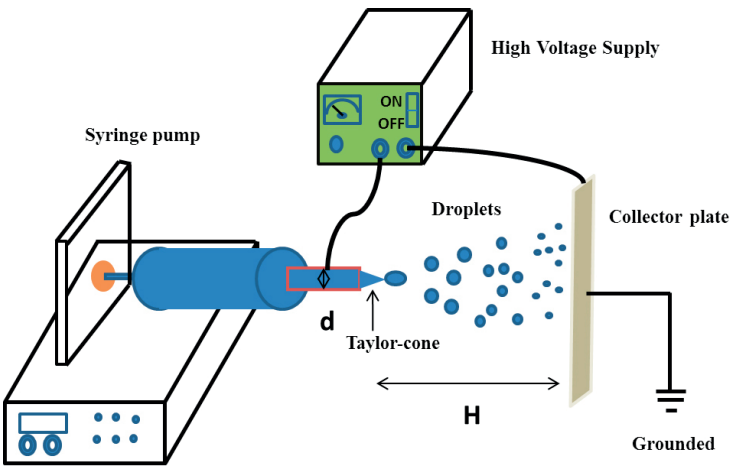

Figure 1. Schematic diagram of the electrospray equipment

The morphology of the as-sprayed CL-20 particles was studied using a field-emission scanning electron microscope (SEM; S4800, Hitachi, Tokyo, Japan). The as-sprayed CL-20 particles collected on the aluminum foil were sputter-coated with gold before SEM observation. The diameter of the particles and the size distributions were determined from the SEM images by using IMAGE PROPLUS software. More than 100 particles were selected for each sample to calculate the average diameters. In-depth transmission electron microscopy (TEM, Tecnai, F30, FEI, USA) was conducted to check whether the as-sprayed particles were agglomerated. X-ray diffraction (XRD) and Fourier-transform infrared spectroscopy (FTIR) were used to test the as-sprayed CL-20 particles using Bruker AXS D8 and NICOLET6700 FTIR instruments, respectively. An HGZ-1 impact instrument and a WM-1 friction instrument were used to measure the mechanical sensitivity of the CL-20 samples. The tests were conducted in the same way as previously reported [2]. The impact sensitivity result was expressed as the H_{50} value (the height required to cause 50% of explosions stimulated by a 2.5 kg hammer). The friction sensitivity was expressed as the explosive probability (P, which was the percentage of explosions stimulated by the pendulum scraped across the sample); the pressure was 2.45 MPa, and the swing angle was 80°. Each sample was tested 25 times to obtain the average value of H_{50} and P. The densities of both the raw and the as-sprayed CL-20 were determined using a Model 3H-2000TD1 automatic true density analyzer. The thermal decomposition properties of both the raw CL-20 and the as-sprayed particles were tested using a differential scanning calorimeter (Netzsch STA 449F, German). The heating rates were fixed at 5 °C/min, 10 °C/min, 15 °C/min and 20 °C/min, ranging from 30 °C to 400 °C.

3 Results and discussion

3.1 Morphologies of the particles

The as-sprayed CL-20 particles are shown in Figure 2. Acetone, ethyl acetate, and a miscible solvent mixture of acetone and ethyl acetate were selected to dissolve CL-20 for the preparation of the precursor solution. Experimental conditions were optimized for the preparation of uniformly sized and distributed particles.

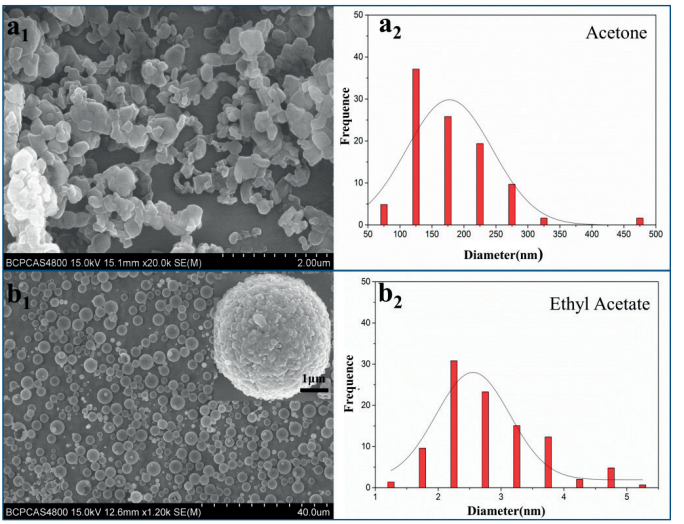

Figure 2. Morphology and size distribution of the as-sprayed CL-20 particles, (a_1, a_2) acetone as solvent, (b_1, b_2) ethyl acetate as solvent. The experimental conditions were: H = 120 mm, d = 0.58 mm, c = 20 mg/ml, U = 6.0 kV

Figure 2(a_1) showed that when acetone was used as the solvent, the CL-20 particles obtained were not uniformly spherical. However, some spherical particles were observed. The particles ranged in size from tens of nanometers to hundreds of nanometers and seemed to have a nearly normal distribution, as shown in Figure 2(a_2). The average size of the particles was calculated to be 177.4 nm by measuring almost 100 particles with IMAGE PROPLUS. Figure 2(b_1) showed that when ethyl acetate was used as the solvent, most of the CL-20 particles obtained were spherical. The particles ranged in size from submicron to several microns and seemed to have a normal distribution, as shown in Figure 2(b_2). The average size of the particles was calculated to be 2.8 μm by measuring approximately 100 particles. An amplified image for a single particle is shown in Figure 2(b_1), which shows that th spherical particles were aggregates of smaller particles instead of single particles.

Compared with the other spray-drying method, electrospray can produce narrow distribution fine droplets from a conductive solution, due to the imbalance of an electrostatic force and a surface tension force being applied on large droplets at the tip of the metallic nozzle [13]. Of the various spraying modes, such as dripping mode, cone-jet mode, and multi-jet mode, that exist [14], the cone-jet mode is preferred for preparing fine monodispersed and nanometer-

sized particles. The electrospray process was conducted under different conditions, such as different solution properties (*e.g.* electric conductivity, dielectric constant, and viscosity) and parameters (*e.g.* potential difference, flow rate, solution concentration, and working distance between the two poles) [15]. The primary experimental conditions to obtain the cone-jet were achieved by changing the voltage, working distance, nozzle diameter, and the type of solvent. The effects of using different types of solvent on the morphology of the particles are discussed in detail.

Initially, an appropriate selection of the parameters was important for establishing the cone-jet mode. It is well known that the formation of the cone-jet mode is a function of the five dominating process parameters and solution properties [16]. These process parameters included the inner nozzle diameter (d), working distance (H), flow rate (Q), initial solution concentration (c), and working voltage (U). The solution properties considered were surface tension, dielectric constant, boiling point, and viscosity. Figure 3(a) shows the range of the working voltage required to form the cone-jet at different working distances.

The experiments were first performed with CL-20 in acetone at 20 mg/cm^3. The inner diameter of the nozzle was 0.58 mm, and the flow rate was 1 cm^3/h. The maximum working distance was limited by the experimental arrangement to 120 mm. Figure 3(a) shows that in order to obtain the Taylor-cone, the applied working voltage had to be increased as the working distance was increased. In this case, the working voltage had to be not less than 4 kV or higher than 6 kV to form the cone-jet mode at a working distance of 50 mm. Only an intermittent jet with larger droplets at the tip of the capillary was obtained when the working voltage was smaller than the limiting value of U_{min}. Similarly, the cone-jet broke into several individual cones when the working voltage was larger than U_{max} because of the high surface charge density at the nozzle tip. Over the operational interval (between U_{max} and U_{min}), a single continuous jet called the cone-jet mode was built to form fine, monodispersed droplets. Furthermore, the relationship between the working voltage and the working distance was not linear. Instead, the operational interval value of the working voltage increased faster than the working distance. The operation interval value of the working voltage was 1.98 kV, 2.14 kV, 2.45 kV, 2.69 kV, 2.77 kV, 2.87 kV, 2.94 kV and 3.02 kV at working distances of 50 mm, 60 mm, 70 mm, 80 mm, 90 mm, 100 mm, 110 mm and 120 mm, respectively. Figure 3(b) shows the maximum and minimum voltages for establishing the stable cone-jet mode according to the inner nozzle diameter under the following conditions: 20 mg/cm^3 of CL-20 in acetone, working distance 80 mm, flow rate 1 cm^3/h. A larger inner diameter of the nozzle caused a higher voltage to be required

to form a continuous jet. This could be attributed to the fact that for a larger nozzle, the diameter of the cone would be larger, which would result in greater surface tension; thus, more electrostatic force would be required to overcome the surface tension. The value of the operational interval was approximately 3 kV for all of the selected nozzles. The experiments were performed under the abovementioned conditions.

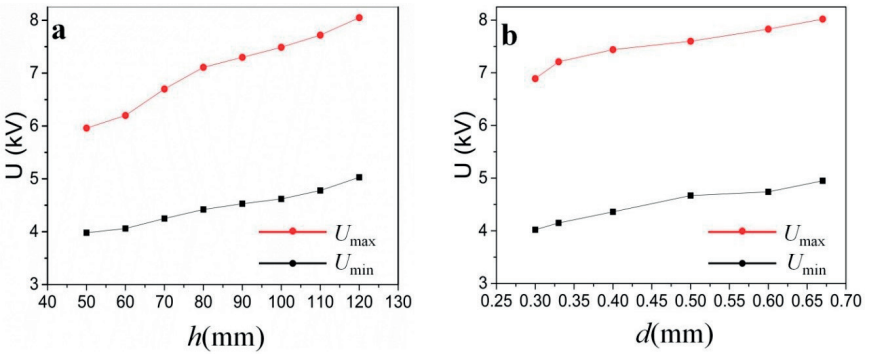

Figure 3. The limiting voltage range to form the cone-jet at different working distances (a) and with different inner diameters of the nozzle (b); *h* is the working distance, *d* is the inner diameter of the nozzle

The properties of the precursor solution was significantly affected by the solvent type required to dissolve CL-20. The properties of ethyl acetate and acetone are listed in Table 1.

Table 1. Properties of the solvents [17]

Solvent	Solubility [g/100 g solvent]*	Boiling point [°C]	Evaporation rate**	Viscosity [cP]	Surface tension [mN/m]
Acetone	94.6-97.1	56.2	1120	0.316	23.7
Ethyl acetate	42.97-45.0	77.1	615	0.449	23.75

Note: * – The solubility of CL-20 was calculated at 25 °C. ** – The evaporation rate was higher than that of n-butyl acetate.

As the particle size of CL-20 prepared using acetone as the solvent differed considerably from that of ethyl acetate, the properties of the precursor solutions were studied, particularly from the viewpoints of conductivity and viscosity. A mixture of acetone and ethyl acetate was used as the solvent in the volume ratios of $V_A/V_T = 0.2$, 0.4, 0.6, and 0.8, where V_A is the volume of acetone added

to the mixture and V_T is the total volume of the mixture. The CL-20 particles made when using the mixed solvents are shown in Figure 4.

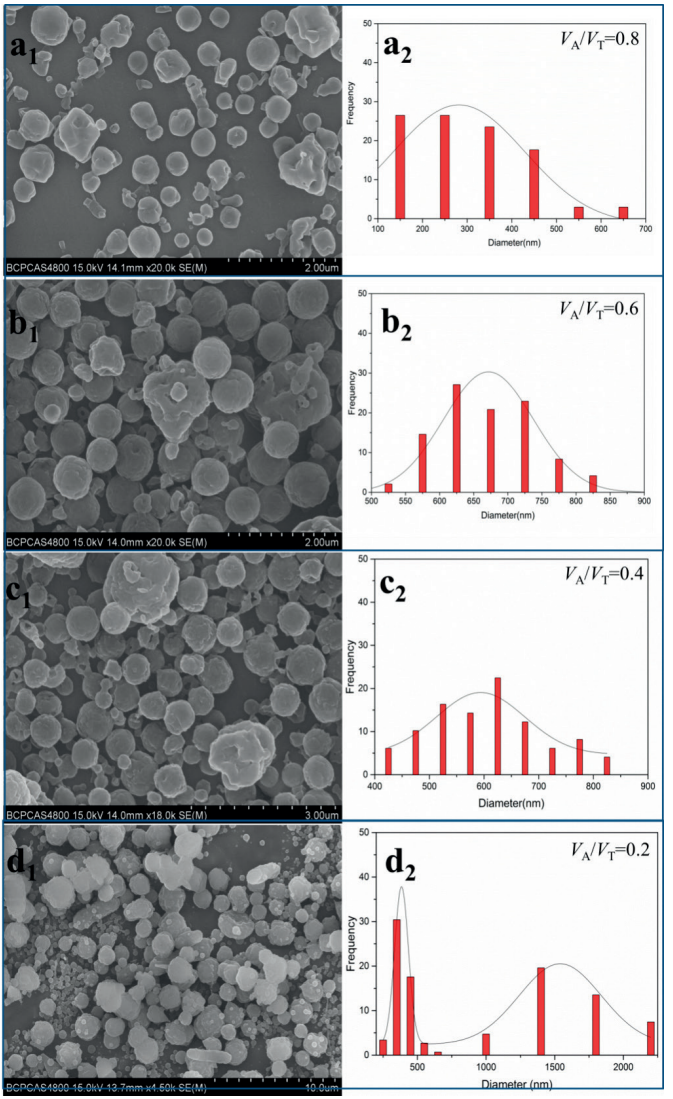

Figure 4. Morphology and size distribution of CL-20 particles obtained with different contents of acetone in the mixed solvents, (a_1, a_2) $V_A/V_T = 0.8$, (b_1, b_2) $V_A/V_T = 0.6$, (c_1, c_2) $V_A/V_T = 0.4$, (d_1, d_2) $V_A/V_T = 0.2$. The other experimental conditions were fixed at: H = 120 mm, d = 0.58 mm, c = 20 mg/cm^3, U = 6.0 kV

Compared to using pure acetone as the solvent, as shown in Figure 2(a_1), the addition of 20% ethyl acetate led to a uniform size distribution of the particles, as shown in Figure 4(a_1). The average particle size of this sample was 321.5 nm. By contrast, adding 20% acetone to ethyl acetate led to a bimodal distribution, several hundred nanometers and several microns. The average sizes of the samples were 525.8 nm and 608.5 nm when the acetone content was 60% and 40%, respectively, in the mixed solvent. The average sizes of all six samples mentioned are shown in Figure 5.

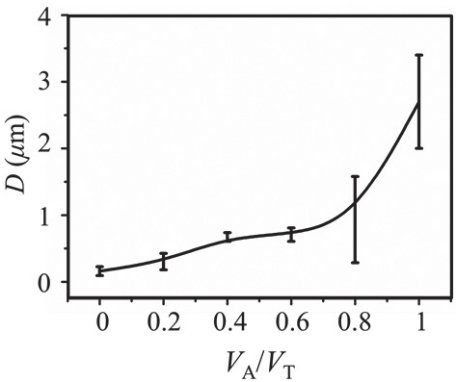

Figure 5. The average sizes of the samples when using pure acetone, acetone content of 80%, 60%, 40% and 20%, and pure ethyl acetate as the solvent

Many researchers have reported that the particle size depended mainly on the size of the droplets during the spray-drying process [18, 19], although the structure and the morphology might be affected by the drying kinetics. The viscosity, conductivity, and surface charge of the precursor solution should be taken into account in the droplet formation process [20]. As the experimental conditions were fixed at H = 120 mm, d = 0.58 mm, c = 20 mg/cm^3, and U = 6.0 kV in all of the six tests, the main reason for the differences in the morphologies and sizes was thought to be the use of different solvents. The most important properties of the solvents that affected the electrospray process were surface tension, conductivity, and viscosity. As the values of the surface tension of acetone and ethyl acetate were very close to each other (26.29 mN/m and 26.26 mN/m, respectively, at 20 °C), the surface tension of the precursor solution was not tested. The conductivity and the viscosity of the precursor solutions were measured as shown in Figure 6.

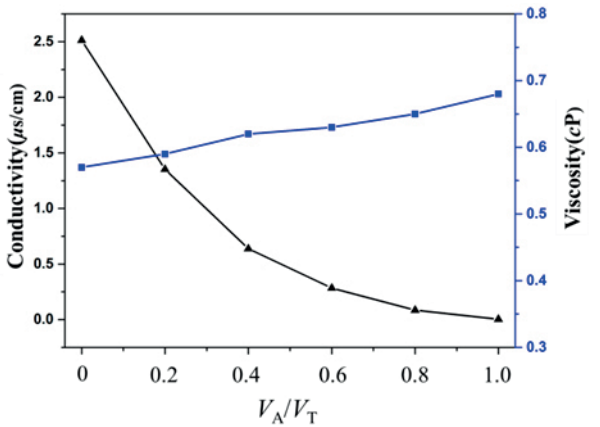

Figure 6. Conductivity and viscosity of the precursor solutions

Figure 6 shows that the viscosity of the precursor solution increased very slowly with the increase of acetone in the mixed solvent, while the conductivity decreased sharply from 2.48 ms/cm to 0.16 ms/cm when the mixed solvents contained more acetone. Therefore, the differences in the size distribution of the samples could be attributed to conductivity.

As the surface of the large particles appeared to be rough, SEM was performed on the pretreated samples to obtain more information about the internal structure, and TEM was performed to check whether the particles were aggregates of smaller particles. The samples shown in Figure 2(a_1) were first frozen and slightly crushed before SEM. The SEM and TEM results of the samples are shown in Figure 7.

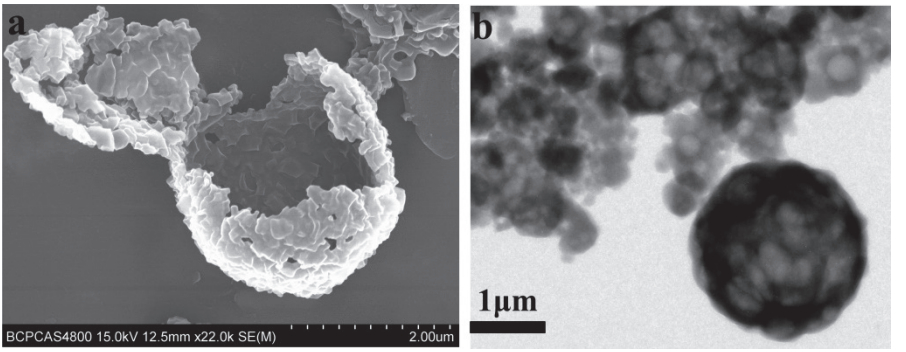

Figure 7. SEM and TEM of the CL-20 particles obtained using ethyl acetate as solvent, (a) SEM image, (b) TEM images

In general, the particle size was mainly affected by the spray process, while the morphology and the structure of the particles depended mainly on the kinetics of crystallization and the kinetics of drying. Figure 7(a) clearly shows that the spheres of the CL-20 particles were hollow layered when pure ethyl acetate was used as the solvent. The particle layers consisted of smaller particles measuring several hundred nanometers. The TEM image also shows that the large particles were aggregates of smaller particles. A hollow layered structure was obtained in the cases of both electrospray [21, 22] and spray-drying [19]. The formation of hollow layered spheres was controlled by the drying process. During flight, the solvent volatilized from the surface of the droplet and an over-saturated solution formed close to the droplet surface. When the drying process was sufficiently fast, a large number of small particles were generated; they aggregated on the surface of the droplet to form a shell. When the drying process was not sufficiently fast, the smaller particles were not fast enough to form the shell. Thus, the droplet would break into smaller droplets during accelerated flight. The formation of the single particles was controlled by the crystallization process. A crystal seed would be formed first after the formation of a droplet. Then, upon volatilization of the solvent, the crystallization process continued to form a larger particle. Meanwhile, if the crystallization process was sufficiently fast, considerably larger single particles (measuring several microns) might be obtained. The primary particle of the aggregated layer was several hundreds of nanometers in size, which was close to the particle sizes shown in Figure 2(a_1) and Figure 4(a_1). Thus, it was speculated that the smaller particles were almost solid spheres.

3.2 Crystal phase

Under normal conditions, the four experimentally isolated polymorphs of CL-20 are the α-, *β*-, γ-, and ε- phases. The stability of the isolated polymorphic forms decreased in the following order: $\varepsilon > \gamma > \alpha > \beta$. The ε- phase is the most attractive as an energetic material because of its higher density (2.044 g/cm^3) and lower sensitivity compared to the other three phases. However, ε-CL-20 could not be directly produced in many synthetic techniques, particularly in the case of a relatively fast crystallization process [23-27]. *β*-CL-20 is usually obtained during the early stages of crystallization [28].

As, in the present case, the crystallization process of CL-20 was completed within a short time during the flight of the droplet from the nozzle to the metal plate, the CL-20 phase should be of the *β* form. Solvent and anti-solvent techniques are usually used for the recrystallization of CL-20 to obtain the ε phase [29, 30].

XRD and infrared scanning (IR) were performed on the raw CL-20 and the typical as-sprayed CL-20. The results are shown in Figure 8.

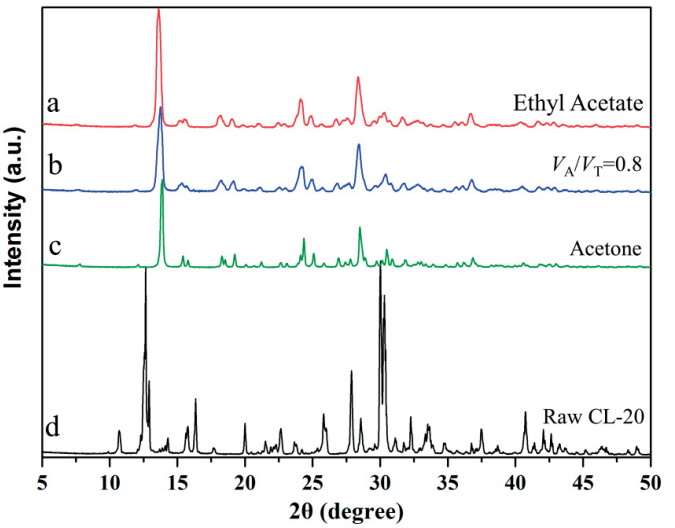

Figure 8. XRD patterns of raw CL-20 and as-sprayed CL-20 particles. All polymorph measurements were performed on a Bruker D8 Advance. The 2θ was measured from 5° to 50° in increments of 0.02°/0.1 s

Compared to the XRD patterns of pure ε- and *β*-CL-20 (PDF#: 050-2045 and 052-2432), Figure 8 shows that the raw material was ε-CL-20 and all of the tested as-sprayed samples were *β*-CL-20. The IR images showed the same result, as illustrated in Figure 9. Therefore, as *β*-CL-20 is usually considered to be a metastable phase, solvent and anti-solvent or other techniques could be used for the recrystallization of the CL-20 to obtain the ε phase if required [29].

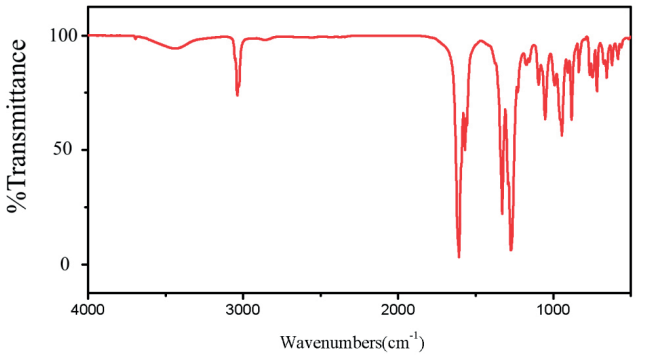

Figure 9. FTIR of typical CL-20 particles prepared from the solutions in acetone, ethyl acetate and the mixed solvent of $V_A/V_T = 0.8$

3.3 Mechanical sensitivity and density

The mechanical sensitivity and the density were determined for the raw CL-20 (HC), the as-sprayed nano CL-20 (NC, shown in Figure 3(a_1)), and the micron hollow CL-20 (MC, shown in Figure 3(b_1)). MC was gently ground to small particles in a mortar before the tests. The results showed that the densities of NC and MC were really close, 1.97 g/cm^3 and 1.96 g/cm^3, respectively. This also indirectly proved that the hollow layered micron CL-20 consisted of primary particles, which were also solid particles. Compared to the density of HC (2.03 g/cm^3), the decrease in the density values were mainly caused by the changes in the crystal phase from ε and *β*.

The mechanical sensitivity results are presented in Table 2. For the impact sensitivity, a large value of H_{50} implied that the sample was less sensitive, *i.e.* safer. The H_{50} of NC was 24.2 cm, which was 59.2% higher than that of HC. The H_{50} of MC was 19.8 cm, which was 30.2% higher than HC. For the friction sensitivity, a smaller value of P implies that the sample was less sensitive, *i.e.* safer. The P values of NC and MC had decreased by 21.1% and 13.2%, respectively, compared to HC. The change in the sensitivity values with a decrease in the particle size has been explained by the hotspots theory in another report [2]. The smaller particle size led to better mechanical sensitivity as the phase change from ε *to β* increased the mechanical sensitivity [28]. Therefore, the change in particle size had a greater influence than the crystal phase change for NC and MC. The difference in sensitivity between NC and MC was mainly attributed to the grinding process. The sharp edges of the broken particles would create hotspots under the action of mechanical stimuli.

Table 2. Mechanical sensitivity of the CL-20 samples

CL-20 sample	H_{50} [cm]	P [%]
HC	15.2	76
NC	24.2	60
MC	19.8	66

3.4 Thermal decomposition properties

Thermal decomposition experiments on CL-20 were carried out to study its thermal stability and reactivity. The DSC patterns of the raw CL-20 and the as-sprayed CL-20 (shown in Figure 3(a_1)) are shown in Figure 10.

Figure 10 shows two reactions for the raw CL-20 during the heating process, compared to only one reaction for the as-sprayed CL-20. The first reaction of the raw CL-20 occurred in the temperature range of 165 °C to 175 °C, corresponding to the solid phase transition from ε to γ [31]. The main reaction occurred after the phase transition, corresponding to the thermal decomposition reaction. The exothermic peak temperature for the raw CL-20 heated at the rate of 5 °C/min was approximately 237.3°C, which was about 15.1 °C higher than that of the as-sprayed CL-20.The exothermic peak temperature of the thermal decomposition reaction increased as the heating rate was increased. A number of studies have reported that for different phases of CL-20, the thermal decomposition reaction started at really close temperatures. The main reason for the temperature difference between the two samples here was the difference in particle size. This was consistent with previous results [30].

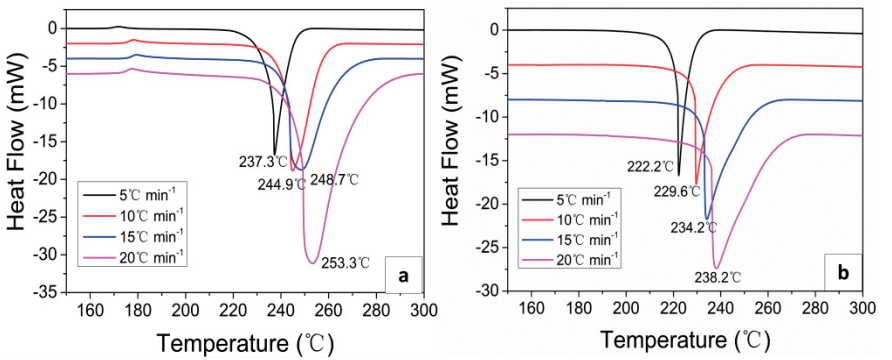

Figure 10. DSC curves of raw CL-20 and the as-sprayed CL-20, at heating rates of 5 K/min, 10 K/min, 15 K/min and 20 K/min, (a) raw CL-20, (b) as-sprayed CL-20

Based on the peak temperatures of the thermal decomposition reactions at the four heating rates, the kinetic parameters (activation energy E_a, and pre-exponential A) were calculated using the Kissinger method, which is based on the shift of the peak temperature at different heating rates [32]. In Equation (1), $\ln(\beta_i/(T_{pi})^2)$ has a linear relationship with $1/T_{pi}$. By plotting $\ln(\beta_i/(T_{pi})^2)$ against $1/T_{pi}$, a straight line was obtained by linear fitting, as shown in Figure 11. The values of E_a and A were calculated from the slope ($-E/R$) and the intercept $\ln(AR/E_a)$.

$$\ln(\beta_i/(T_{pi})^2)=\ln(AR/E_a) - E_a/(RT_{pi}) \quad (1)$$

where β_i is the heating rate in K/min, T_{pi} is the temperature of the exothermic peak at the heating rate of β_i measured in K. A is the pre-exponential factor in units of s^{-1}. E_a is the activation energy in J/mol, and R is the gas constant with a value of 8.314 J/(mol·K).

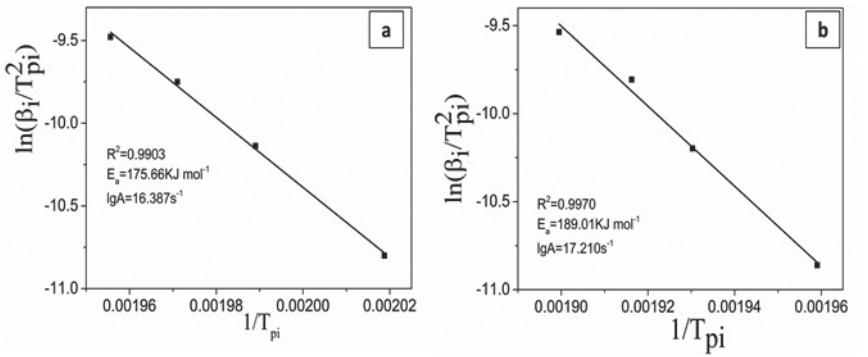

Figure 11. The kinetic parameters of thermal analysis, (a) as-sprayed CL-20, (b) raw CL-20

Through liner fitting of four points that included the X coordinate, Y coordinate, $1/(T_{pi})$ and $\ln(\beta_i/(T_{pi})^2)$, the activation energy E_a was determined to be 175.66 kJ/mol for the as-sprayed CL-20, and 189.01 kJ/mol for the raw CL-20, showing that the as-sprayed CL-20 decomposed more easily than the raw CL-20.

4. Conclusions

Nano- and micron-sized spheres of CL-20 could be continuously fabricated by electrospray. The morphology and the particle size mainly depended upon

the properties of the precursor solution, particularly the conductivity. Solid particles on the scale of several hundred nanometers could be obtained when acetone or a mixture of acetone and a little ethyl acetate was used as the solvent. However, when ethyl acetate was used as the solvent, hollow layered spherical particles, measuring in the range of sub-micron to several microns, were obtained. The layers of the hollow spheres were an agglomeration of the primary particles, measuring in nanometers. The as-sprayed samples were of the β form as revealed by XRD and FTIR. Thus, the density of the as-sprayed CL-20 was 1.97 g/cm^3, which was lower than that of the raw CL-20. The impact sensitivity and the friction sensitivity decreased by 59.2% and 21.1%, respectively, for the solid smaller particles as compared to the raw CL-20. The activation energy for thermal decomposition of the as-sprayed CL-20 was 175.66 kJ/mol and 189.01 kJ/mol for the raw CL-20, showing that the as-sprayed CL-20 decomposed more easily than raw CL-20.

References

[1] Samudre, S. S.; Nair, U. R.; Gore, G. M. Studies on an Improved Plastic Bonded Explosive (PBX) for Shaped Charges. *Propellants Explos. Pyrotech*. **2009**, *34* (2): 145-150.

[2] Guo, X.; Ouyang, G.; Liu, J. Massive Preparation of Reduced-sensitivity Nano-CL-20 and its Characterization. *J. Energ. Mater*. **2015**, *33* (1): 24-33.

[3] Wang, J. Y.; Hao, H.; Wen, Z. X. Prefilming Twin-fluid Nozzle Assisted Precipitation Method for Preparing Nanocrystalline HNS and its Characterization. *J. Hazard. Mater*. **2009**, *162*(s 2-3): 842-847.

[4] Hongwei, Q.; Victor, S.; Stasio, A. R. D. RDX-Based Nanocomposite Microparticles for Significantly Reduced Shock Sensitivity. *J. Hazard. Mater*. **2011**, *185*(1): 489-493.

[5] Lee, B. M.; Kim, D. S.; Lee, Y. H. Preparation of Submicron-sized RDX Particles by Rapid Expansion of Solution Using Compressed Liquid Dimethyl Ether. *J. Supercrit. Fluids* **2011**, *57*(3): 251-258.

[6] Li, J.; Brill, T. Nanostructured Energetic Composites of CL-20 and Binders Synthesized by Sol-Gel Methods. *Propellants Explos. Pyro*tech. **2006**, *31*(1): 61-69.

[7] Radacsi, N.; Stankiewicz, A. I.; Creyghton, Y. L. M. Electrospray Crystallization for High-quality Submicron-sized Crystals. *Chem. Eng. Technol*. **2011**, *34*(4): 624-630.

[8] Tapia-Hernández, J. A.; Torres-Chávez, P. I.; Ramírez-Wong, B. Micro- and Nanoparticles by Electrospray: Advances and Applications in Foods. *J. Agric. Food Chem*. **2015**, *63*(19): 4699-4707.

[9] Ju, J.; Yamagata, Y.; Higuchi, T. Thin-film Fabrication Method for Organic

Light-emitting Diodes Using Electrospray Deposition. *Adv. Mater*. **2009**, *21*(43): 4343-4347.

[10] Shi, Y.; Guoqiang, J.; Zachariah, M. R. Electrospun Nanofiber Based Thermite Textiles and Their Reactive Properties. *ACS Appl. Mater. Interfaces* **2012**, *4*(12): 6432-6435.

[11] Wang, H.; Jian, G.; Yan, S. Electrospray Formation of Gelled Nano-aluminum Microspheres with Superior Reactivity. *ACS Appl. Mater. Interfaces* **2013**, *5*(15): 6797-6801.

[12] Hwang, W.; Xin, G.; Cho, M. Electrospray Deposition of Polymer Thin Films for Organic Light-Emitting Diodes. *Nanoscale Res. Lett*. **2012**, *7*(1): 52.

[13] Melgar, V. M. A.; Kwon, H. T.; Kim, J. Direct Spraying Approach for Synthesis of ZIF-7 Membranes by Electrospray Deposition. *J. Membr. Sci*. **2014**, *459*(2): 190-196.

[14] Kwon, H. T.; Kim, J.; Park, J. H. Synthesis and Characterization of Porous $La_{1-x}Sr_xCo_{1-y}Fe_yO_3$ - Membranes Fabricated Using by Electrostatic Spray Deposition. *J. Korean Phys. Soc*. **2009**, *54*(3): 2672-2682.

[15] Radacsi, N.; Stankiewicz, A. I.; Creyghton, Y. L. M. Electrospray Crystallization for High-Quality Submicron-Sized Crystals. *Chem. Eng. Technol*. **2011**, *34*(4): 624-630.

[16] Radacsi, N.; Ambrus, R.; Szunyogh, T. Electrospray Crystallization for Nanosized Pharmaceuticals with Improved Properties. *Cryst. Growth Des*. **2012**, *12*(7): 3514-3520.

[17] Holtz, E. V.; Ornellas, D.; Foltz, M. F. The Solubility of ε-CL-20 in Selected Materials. *Propellants Explos. Pyrotech*. **1994**, *19*(4): 206-212.

[18] Zellmer, S.; Garnweitner, G.; Breinlinger, T. Hierarchical Structure Formation of Nanoparticulate Spray-dried Composite Aggregates. *ACS Nano* **2015**, *9*(11): 10749-10757.

[19] Sloth, J.; Jørgensen, K.; Bach, P. Spray Drying of Suspensions for Pharma and Bio Products: Drying Kinetics and Morphology. *Ind. Eng. Chem. Res*. **2009**, *48*(7): 3657-3664.

[20] Hartman, R. P. A.; Brunner, D. J.; Camelot, D. M. A. Jet Break-up in Electrohydrodynamic Atomization in the Cone-jet Mode. *J. Aerosol Sci*. **2000**, *31*(1): 65-95.

[21] Rasekh, M.; Young, C.; Roldo, M. Hollow-layered Nanoparticles for Therapeutic Delivery of Peptide Prepared Using Electrospraying. *J. Mater. Sci.: Mater. Med*. **2015**, *26*(11): 256.

[22] Radacsi, N., Stankiewicz, A. I.; Creyghton, Y. L. M.; van der Heijden, A. E. D. M.; ter Horst, J. H. Electrospray Crystallization for High-quality Submicron-sized Crystals. *Chem. Eng. Technol.* **2011**, *34*(4): 624-630.

[23] Nielsen, A. T. *Caged Polynitramine Compound.* US Patent 5693794, **1997**.

[24] Latypov, N. V.; Wellmar, U.; Goede, P. Synthesis and Scale-up of 2,4,6,8,10,12-Hexanitro-2,4,6,8,10,12-hexaazaisowurtzitane from 2,6,8,12-Tetraacetyl-4,10-dibenzyl-2,4,6,8,10,12-hexaazaisowurtzitane (HNIW,

CL-20). *Org. Process Res. Dev*. **2014**, *4*(3): 156-158.
[25] Saderson, A. J. *Process for Making 2,4,6,8,10,12-Hexanitro-2,4,6,8,10,12-hexaazatetracyclo-[5.5.0.0^{5,9}0^{3,11}]-dodecane.* US Patent 6391130B1, **2002**.
[26] Hamilton, R. S.; Mancini, V.; Nelson, C.; Dressen, S. Y. *High Temperature Crystallization of 2,4,6,8,10,12-Hexanitro-2,4,6,8,10,12-hexaazatetracyclo-[5.5.0.0^{5,9}0^{3,11}]-dodecane.* US Patent 7288648 B2, **2007**.
[27] Talawar, M. B.; Sivabalan, R.; Polke, B. G. Establishment of Process Technology for the Manufacture of Dinitrogen Pentoxide and its Utility for the Synthesis of Most Powerful Explosive of Today − CL-20. *J. Hazard. Mater*. **2005**, *124*(s 1-3): 153-164.
[28] Xu, J.; Tian, Y.; Liu, Y. Polymorphism in Hexanitrohexaazaisowurtzitane Crystallized from Solution. *J. Cryst. Growth* **2012**, *354*(1): 13-19.
[29] Elbeih, A.; Husarova, A.; Zeman, S. Path to ε-HNIW with Reduced Impact Sensitivity. *Cent. Eur. J. Energ. Mater.* **2011**, *8*(3): 173-182.
[30] Urbelis, J. H.; Swift, J. A. Solvent Effects on the Growth Morphology and Phase Purity of CL-20. *Cryst. Growth Des*. **2014**, *14*(4): 1642-1649.
[31] Zhang, P.; Xu, J. J.; Guo, X. Y. Effect of Additives on Polymorphic Transition of ε-CL-20 in Castable Systems. *J. Therm. Anal. Calorim*. **2014**, *117*(2): 1001-1008.
[32] Kissinger, H. E. Reaction Kinetics in Differential Thermal Analysis. *Anal. Chem*. **1957**, *29*(11): 1702-1706.

Received: December 16, 2017
Revised: December 6, 2018
First published online: December 17, 2018